Journal of Nuclear Materials 390–391 (2009) 250–254

Contents lists available at ScienceDirect

Journal of Nuclear Materials

journal homepage: www.elsevier.com/locate/jnucmat

# Current understanding of divertor detachment: Experiments and modelling

M. Wischmeier [a,*], M. Groth [b], A. Kallenbach [a], A.V. Chankin [a], D.P. Coster [a], R. Dux [a], A. Herrmann [a], H.W. Müller [a], R. Pugno [a], D. Reiter [c], A. Scarabosio [a], J.G. Watkins [d], DIII-D team and ASDEX Upgrade team

[a] Max-Planck-Institut für Plasmaphysik, EURATOM-Association, Boltzmannstr. 2, D-85748 Garching, Germany
[b] Lawrence Livermore National Laboratory, Livermore, California,USA
[c] Institut für Energieforschung, Plasmaphysik, EURATOM Association, Jülich, Germany
[d] Sandia National Laboratory, Albuquerque, NM, USA

ARTICLE INFO

*PACS:*
52.20−j
52.25.Vy
52.30.Ex
52.55.Rk
52.55.Fa

ABSTRACT

A qualitative as well as quantitative simulation of experimentally observed plasma parameters in the detached regime proves to be difficult for several tokamaks. A series of ohmic discharges have been performed in ASDEX Upgrade and DIII-D at as similar as possible plasma parameters and at different line averaged densities, $\bar{n}_e$. The experimental data represent a set of well diagnosed discharges against which numerical simulations are compared. For the numerical modelling the fluid-code B2.5 coupled to the Monte Carlo neutrals transport code EIRENE is used. Only the combination of effects, such as geometry, drift terms, neutral conductance, increased radial transport and divertor target composition explains a significant fraction of the experimentally observed ion fluxes, $\Gamma_t$, to the inner and outer target plates as a function of $\bar{n}_e$ in ASDEX Upgrade. The relative importance of the mechanisms leading to detachment differ in DIII-D and ASDEX Upgrade.



## 1. Introduction

Modelling of partial detachment during burning plasma operation and the corresponding design modifications of the divertor structures in ITER are based on 2*D* fluid–neutrals Monte Carlo codes [1]. The operational window for ITER is limited by an upper upstream separatrix density, $n_e^{sep}$ at which the outer target detaches completely, leading to the density limit. Detachment is defined using the following criteria: The loss of total (sum of static and dynamic) plasma pressure along a field line between an upstream location above the X-point and the target plate is a necessary condition. The release of potential energy during surface recombination brings forward the sufficient condition for detachment, the reduction of the peak ion flux, $\Gamma_t^{pk}$, to the target. In the framework established under the International Tokamak Physics Activity (ITPA) Divertor and SOL working group, experimental data were taken from lower single null Ohmic and L-mode discharges in ASDEX Upgrade and DIII-D at as similar as possible discharge parameters. The ion $\nabla B$ drift was towards the active divertor plates. The discharge parameters cover an ITER relevant SOL collisionality. For ASDEX Upgrade the data compared are taken with graphite (year 2006) and tungsten coated graphite (year 2007) as divertor target material. In DIII-D all plasma facing components, PFCs, are composed of graphite. In both devices at the lowest $\bar{n}_e$ the inner target is initially partially detached reaching complete detachment with increasing $\bar{n}_e$. The outer target remains attached with increasing peak ion flux density, $\Gamma_{ot}^{pk}$, up to a value beyond which detachment occurs, defining the detachment threshold density, $\bar{n}_e^{th}$. Beyond $\bar{n}_e^{th}$ the peak ion flux density decreases with increasing $\bar{n}_e$.

In the past attempts of modelling experimental data quantitatively and qualitatively at both divertor targets simultaneously has proven to be difficult [2]. The SOLPS5.0 code package [3], using the multi fluid code B2.5 coupled to the neutrals Monte Carlo Code EIRENE (version '99) with the option of activating all drift terms is used. The physics implemented in the code package represents the quantitatively best available representation of our current understanding about the individual processes present in the SOL with respect to the plasma part. It compromises with respect to the neutral gas model. The improvements in the gas-radiation model are likely to become relevant only at higher $n_e \times R$ values [4].

## 2. Experiment

Given the present definition for detachment the experimental data concentrate on the ion flux densities at the targets, $\Gamma_t$. The discharge parameters in ASDEX Upgrade and DIII-D were $I_p = 1.0$ MA, $B_T = -2.0$ T, $q_{95} \approx 3.4$ with $\sim 210$ kW additional heating power from neutral beam injection in DIII-D. The total power at medium to high $\bar{n}_e$ into the SOL, $P_{SOL}$, is $\sim 900$—$1100$ kW. In ASDEX Upgrade the cryo pumps were active whereas in DIII-D only the turbo molecular pumps were used. A more detailed description of the

* Corresponding author.
*E-mail address:* marco.wischmeier@ipp.mpg.de (M. Wischmeier).

0022-3115/$ - see front matter © 2009 Elsevier B.V. All rights reserved.
doi:10.1016/j.jnucmat.2009.01.081

experimental observations in DIII-D and ASDEX Upgrade with the graphite tiles at the target can be found in [5,6]. The graphite tiles in the strike point zone were replaced by tungsten coated graphite tiles in ASDEX Upgrade in 2007. The discharges were repeated with as similar as possible plasma conditions and strike point sweeps. Fig. 1 compares the experimental data for the upstream SOL density profiles with (a) medium/low recycling and $\bar{n}_e \approx 2.6 \times 10^{19}$ m$^{-3}$, (b) at $\bar{n}_e \approx 5.0$–$5.5 \times 10^{19}$ m$^{-3}$ prior to detachment and (c) during the detached regime at $\bar{n}_e \approx 6.2 \times 10^{19}$ m$^{-3}$. Detachment occurs around $\bar{n}_e \sim 5.0 \times 10^{19}$ m$^{-3}$ with an $\sim 0.5 \times 10^{19}$ m$^{-3}$ later onset with tungsten coated tiles. At the lowest $\bar{n}_e$ and during detachment $\Gamma_{ot}^{pk}$ is similar (Fig. 1(d and e)), at the detachment threshold density $\Gamma_{ot}^{pk}$ (see also Fig. 4(b)) is slightly higher with tungsten coated targets than without. Spectroscopy reveals that volumetric recombination is present during detachment. The absolute value of the total volumetric recombination cannot be determined due to line integration [7]. Fig. 2 shows the experimental inner and outer target profiles from DIII-D. With increasing $\bar{n}_e$, $\Gamma_{ot}^{pk}$ initially increases and then decreases. In DIII-D $\bar{n}_e^{th}$ is lower, however the fraction of total radiated power reaches $\sim 90\%$ compared to $\sim 65\%$ in ASDEX Upgrade. In both devices the inner target peak ion flux, $\Gamma_{it}^{pk}$, decreases in the strike point region with increasing $\bar{n}_e$ [6]. In ASDEX Upgrade the signals from fixed Langmuir probes in the far SOL indicate a radially increasing $\Gamma_t$ at high $\bar{n}_e$. Tomographic inversion images detect strong line emission of $D_\alpha$ in the far SOL, whilst spectroscopic measurements along the inner heat shield show an atomic influx of $D$ at high $\bar{n}_e$, Fig. 3(a). These data correlate with measurements by a fast pressure gauge in ASDEX Upgrade at the bottom of the inner heat shield [8,9].

## 3. Numerical modelling

The aim of the modelling is to reproduce qualitatively and quantitatively the behavior of $\Gamma_t$ simultaneously at the inner and outer targets as a function of $\bar{n}_e$ for ASDEX Upgrade and DIII-D. The contributors to detachment are thought to be removal of power resulting in a divertor plasma at low temperature in which charge exchange collisions and volumetric recombination processes are active in a large enough volume to remove momentum and ions [10,3]. Grids with $48 \times 18$ cells, based on the experimental magnetic configurations, have been used to represent the closed and open divertor geometries with respect to neutrals, Figs. 3(b) and 6(a).

### 3.1. ASDEX Upgrade

A detailed description of the modelling setup for ASDEX Upgrade with a satisfying agreement to experimental data at the lowest density, $\bar{n}_e \approx 2.6 \times 10^{19}$ m$^{-3}$, can be found in [6]. At $\bar{n}_e \approx 2.6 \times 10^{19}$ m$^{-3}$ $P_{SOL}$ is $\sim 560$ kW and 900 kW at higher $\bar{n}_e$. Starting from the results for the lowest $\bar{n}_e$, $n_e^{sep}$ is increased applying a feedback scheme on the gas puff. For studying the processes in the divertor $n_e^{sep}$ is controlled using a feedback scheme on the gas puff. The data on volumetric processes are based on a collision-radiative model. These data include the possibility of molecular assisted recombination effects (MAR) [11] and elastic collisions between molecules and ions.

As a result in the modelling both $\Gamma_{ot}^{pk}$ and $\Gamma_{it}^{pk}$ increase with rising $n_e^{sep}$, Fig. 4. This is *qualitatively* in contradiction to the experimental observations, Fig. 4(b). Even when resolving the vibrationally excited levels of deuterium molecules using effective energy levels [12] as in [13] no considerable effect of MAR as an ion sink could be found. In the high recycling and detached regimes strong poloidal temperature gradients, $\nabla_\Theta T$, are expected. With the ion $\nabla B$ drift direction towards the outer target the resulting $\mathbf{E}_\Theta \times \mathbf{B}$ drift velocity drives plasma perpendicular to the magnetic field from the LFS to the HFS in regions of $\nabla_\Theta T$. However, as shown in Fig. 4(a) no decreasing $\Gamma_{it}^{pk}$ as a function of $\bar{n}_e$ is observed. By de-

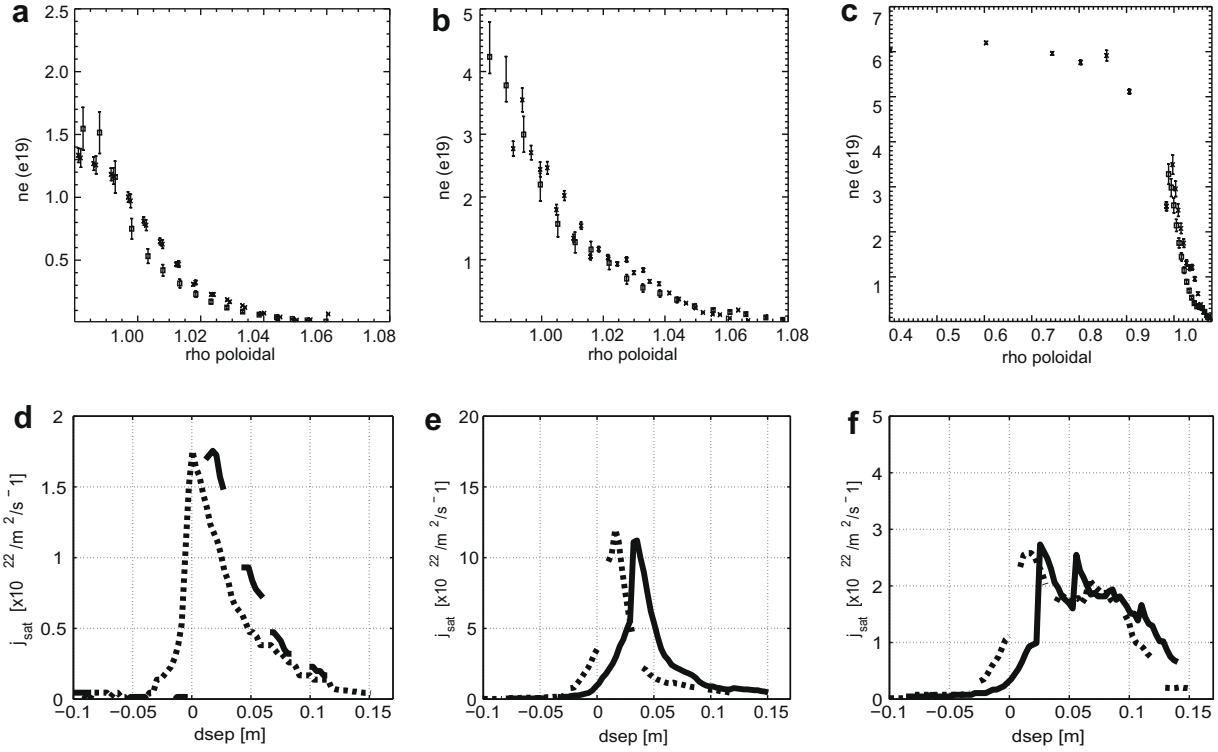


**Fig. 1.** Upstream density profiles (top row) for discharges with $C$ (×) and $W$ (□) target plates and corresponding ion saturation flux profiles (bottom row) at the outer target; dashed line for $C$ and a solid line for $W$ for different $\bar{n}_e$; first column (a and d) at $\bar{n}_e \approx 2.6 \times 10^{19}$ m$^{-3}$, second column (b,e) at $\bar{n}_e \approx 5.5 \times 10^{19}$ m$^{-3}$ and last column (c,f) at $\bar{n}_e \approx 6.5 \times 10^{19}$ m$^{-3}$.

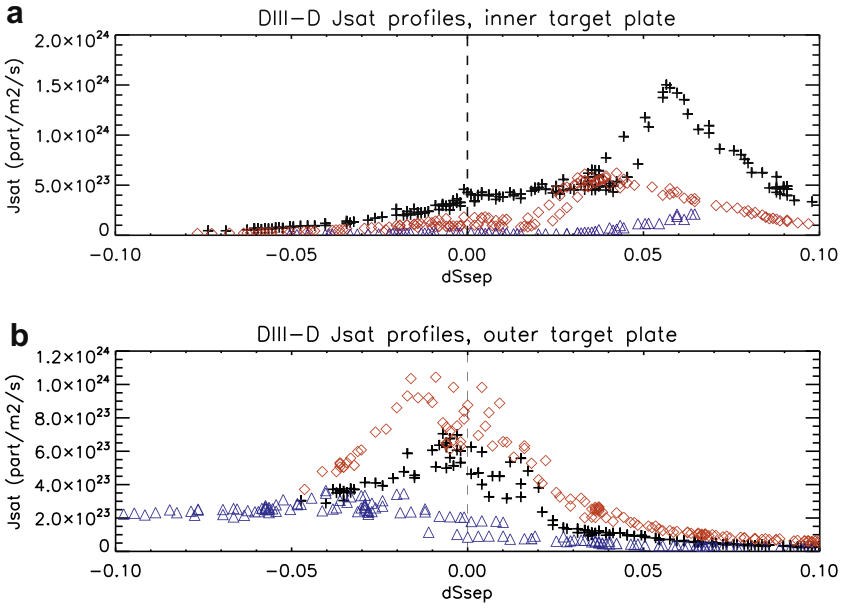


**Fig. 2.** Ion saturation current profiles along the inner (a) and outer targets (b) of DIII-D at three different $\bar{n}_e$ ('◇' $\bar{n}_e \approx 2.6 \times 10^{19} m^{-3}$,'+' $\bar{n}_e \approx 3.0 \times 10^{19}$ m$^{-3}$,'△' $\bar{n}_e \approx 3.9 \times 10^{19}$ m$^{-3}$.

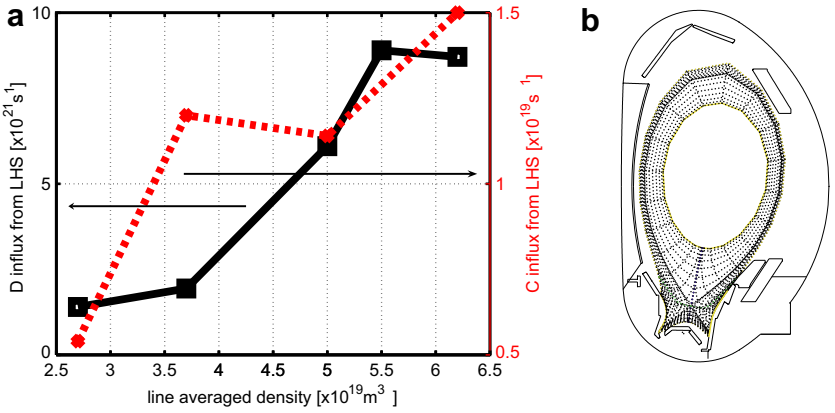


**Fig. 3.** The integral particle $D$ and $C$ influx from the inner lower heat shield of ASDEX Upgrade as a function of $\bar{n}_e$, (a) and the computational grid for ASDEX Upgrade (#21303@3.2 s) (b).

fault the neutral conductivity below the dome is not limited, Fig. 3(b). At low $\bar{n}_e$ a neutral pressure gauge in the outer divertor target plate, [8], measures a neutral flux by a factor $\sim 3$ smaller than below the dome. Thus the conductivity for neutrals below the dome is limited and was unknown during the simulations. As a mock up a baffle with a small gap is simulated below the dome and the implications are tested. As expected without activated drift terms no improvement is seen, see also [14]. With all the drift terms activated, Fig. 4(a) shows how then $\Gamma_{it}^{pk}$ does not increase and Fig. 4(b) shows that $\Gamma_{ot}^{pk}$ is now even lower than the experimental data. Including the impurity influx measured from spectroscopy along the inner heat shield as an external impurity source into the model does not decrease $\Gamma_{it}^{pk}$. The results do not imply that the code package does not model detachment as such. The total pressure loss along a field line between the outer midplane and the inner target can be more than a factor of 10 and despite the increase of $\Gamma_{ot}^{pk}$ the total pressure is reduced. In the modelling the high recycling fluxes along the inner heat shield are absent and a further assumption is introduced. The perpendicular particle diffusion coefficient, $D_\perp$, has been increased in the far SOL from 1 m$^2$/s to 20 m$^s$/s and above. This increase does not affect the profiles of $\Gamma_t$ considerably at low $n_e^{sep}$. At the highest $\bar{n}_e$ a tendency towards the experimentally observed increased particle fluxes in the far SOL and, as shown in Fig. 5, a reduced $\Gamma_{it}^{pk}$ is seen, which does not appear on the LFS. The integral value however only decreases marginally. Even though the activation of drift terms does reduce $\Gamma_{it}^{pk}$ further it cannot be shown that such enhanced particle fluxes are absent in the far SOL in the absence of activated drift terms.

### 3.2. DIII-D

In DIII-D, Fig. 6(a), the estimate is $P_{SOL} \sim 800$ kW. Experimentally at the lowest $\bar{n}_e$ the upstream $n_e$ and $T_e$ profiles are similar in DIII-D to ASDEX Upgrade [5]. Consequently the same radial profile for perpendicular diffusive transport coefficients as for ASDEX Upgrade is used. However, testing different radial profiles of $\chi_e$, $\chi_i$ and $D_\perp$ it was not possible to match simultaneously a $T_e^{sep}$, of $\sim 50$ eV and $n_e^{sep} \approx 0.8 \times 10^{19}$ m$^{-3}$ for a given $P_{SOL}$ in the margin of the experimental error bars, resulting in $T_e^{sep} \approx 60$—65 eV. The modelling of L-mode discharges for DIII-D may be expected to be

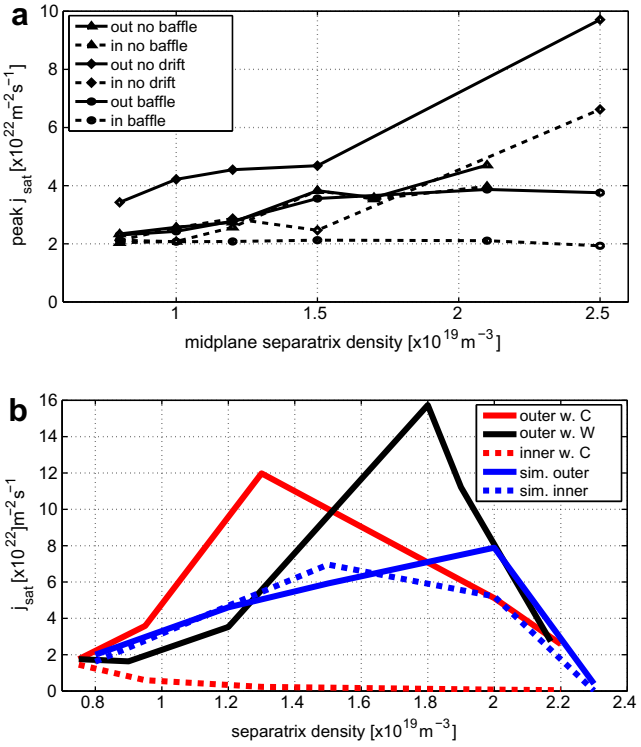


**Fig. 4.** Simulated $\Gamma_t^{pk}$ showing the effect of reduced neutral conduction with a mock up baffle and the effect of drifts (a) and comparison with experiment (b) including drifts and the mock up baffle with $P_{SOL} = 560$ kW at lowest $\bar{n}_e$ and 900 kW at higher $\bar{n}_e$.

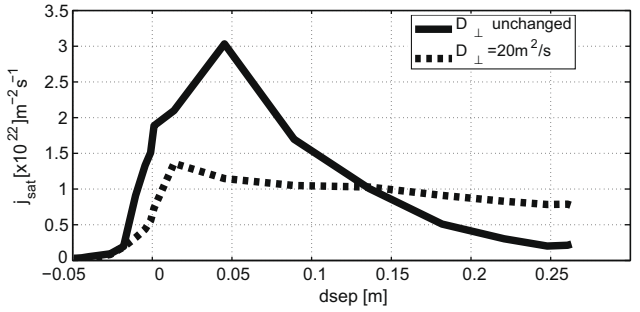


**Fig. 5.** Radial ion flux profiles at the inner target with and without increased SOL transport at $n_e^{sep} = 2.2 \times 10^{19}$ m$^{-3}$.

simpler because less known parameters such as the sub-dome conductance for neutrals or the effective pumping albedo are absent. The treatment using all drift terms activated proved to be numerically challenging and fully converged simulations with all drift terms active are not available. Fig. 6(b) illustrates the major discrepancies between the modelling and the experimental data for $\Gamma_t^{pk}$, where $i\Gamma_{it}^{pk}$ does not decrease as in experiment and $\Gamma_{ot}^{pk}$ remains larger than the experimental value at all $n_e^{sep}$. Experimentally with increasing $\bar{n}_e$ and recycling at the main chamber wall, MCW, a higher impurity influx is expected from the MCW [15]. In the model only neutrals reaching the MCW sputter and the effect of the impinging ion flux can only be taken into account by increasing $Y_{chem}$ for MCW components. This effect reduces $\Gamma_t^{pk}$ for higher $\bar{n}_e$, Fig. 6, but not sufficiently when comparing with experiment. In the code detachment at the outer target occurs at lower $n_e^{sep}$ than for ASDEX Upgrade. This however might be pure coincidence of not reproducing the experimental background plasma.

## 4. Conclusions

Divertor detachment, as such, is simulated using code packages such as SOLPS. However, the experimental in-out asymmetry of $\Gamma_t$ in ohmic/L-mode discharges as a function of $\bar{n}_e$ is not reproduced even with all drift terms activated. The simulated asymmetry decreases with increasing $P_{SOL}$. Detachment is quantitatively and qualitatively not understood if common assumptions are made. The additional assumption of a limited neutrals conductivity below the dome combined with activating all drift terms reduces $\Gamma_{ot}^{pk}$ for high $n_e^{sep}$ to values even lower than experimental data, without affecting results at the lowest $n_e^{sep}$. Drift effects by themselves seem insufficient to explain the divertor asymmetries even though experimentally a change of ion $\nabla\mathbf{B}$ direction alters the degree of asymmetry [16,17]. It cannot be proven that strong perpendicular transport in the far SOL is important for the divertor conditions at the inner target with the model. A grid expanding further out into the SOL is necessary for such an assessment. Detachment in DIII-D can be a consequence of impurity influx from the MCW and the mismatch between simulations and experimental data for DIII-D is likely to be larger due to the open divertor and the neutral fluxes between the two volumes.

## Acknowledgements

This work was performed with support by the Intra-European Fellowship (EURATOM) and the auspices of the US Department of Energy by Lawrence Livermore National Laboratory under Contract

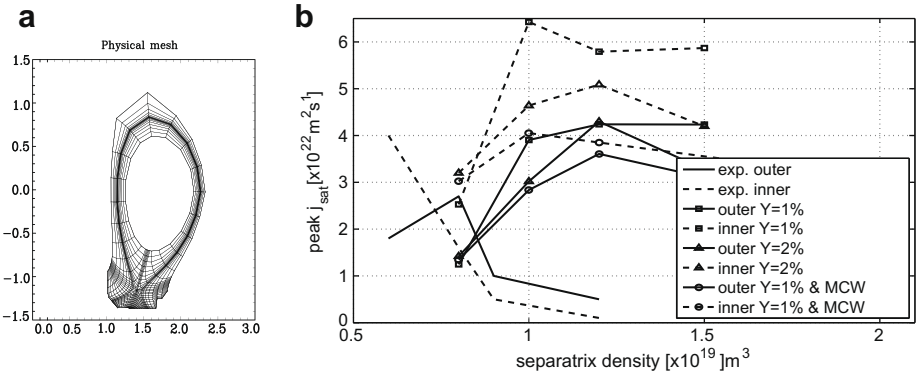


**Fig. 6.** Computational grid for *DIII – D* (a) and comparison of experimental and simulated peak ion fluxes for the outer (solid line) and inner (dashed line) using $Y_{chem} = 1\%$ (□), 2% (△) at the targets and additionally $Y_{chem} = 10\%$ (o) from the MCW as a function of $n_e^{sep}$ for DIII-D.

DE-AC52-07NA27344 and by Sandia National Laboratory under Contract DE-AC04-94AL85000.

## References

[1] Progress in the ITER Physics Basis, Nucl. Fus. 47 (6) (2007) S1.
[2] A.V. Chankin et al., J. Nucl. Mater. 390–391 (2009) 319.
[3] R. Schneider et al., Contribution Plasma Phys. 40 (3–4) (2000) 328.
[4] V. Kotov et al., Contribution Plasma Phys. 46 (7–9) (2006) 635.
[5] M. Groth et al., ECA 31F (2007) P1039.
[6] M. Wischmeier et al., Contribution Plasma Phys. 48 (1–3) (2008) 249.
[7] R. Pugno et al., 27th EPS Conference on Controlled Fusion an Plasma Physics, Budapest, 2000, Europhysics Conference Abstract, vol. 24B, 2000, p. 1168.
[8] A. Scarabosio et al., J. Nucl. Mater. 390–391 (2009) 494.
[9] K. McCormik et al., J. Nucl. Mater. 390–391 (2009) 465.
[10] S.I. Krasheninnikov et al., Phys. Lett. A 214 (1996) 285.
[11] S.I. Krasheninnikov et al., Phys. Plasmas 4 (5) (1997) 1638.
[12] M. Wischmeier et al., Contribution Plasma Phys. 44 (1–3) (2004) 268.
[13] U. Fantz et al., J. Nucl. Mater. 290–293 (2001) 367.
[14] E. Tsitrone et al., Contribution Plasma Phys. 44 (1–3) (2004) 241.
[15] D.G. Whyte et al., Nucl. Fus. 41 (2001) 1243.
[16] A. Huber et al., J. Nucl. Mater. 337–339 (2005) 241.
[17] R. Pitts et al., J. Nucl. Mater. 337–339 (2005) 146.